ACS Photonics

ACS Editors' Choice

Letter

pubs.acs.org/journal/apchd5

Terms of Use

Third Harmonic Mechanism in Complex Plasmonic Fano Structures

Bernd Metzger,*[,†] Thorsten Schumacher,[†,‡,§] Mario Hentschel,[†,‡] Markus Lippitz,[†,‡,§] and Harald Giessen[†]

[†]4th Physics Institute and Research Center SCoPE, University of Stuttgart, Pfaffenwaldring 57, 70569 Stuttgart, Germany

[‡]Max Planck Institute for Solid State Research, Heisenbergstr. 1, 70569 Stuttgart, Germany

[§]Experimental Physics III, University of Bayreuth, Universitaetsstr. 30, 95447 Bayreuth, Germany

Supporting Information

ABSTRACT: We perform third harmonic spectroscopy of dolmen-type nanostructures, which exhibit plasmonic Fano resonances in the near-infrared. Strong third harmonic emission is predominantly radiated close to the low energy peak of the Fano resonance. Furthermore, we find that the third harmonic polarization of the subradiant mode interferes destructively and diminishes the nonlinear signal in the far-field. By comparing the experimental third harmonic spectra with finite element simulations and an anharmonic oscillator model, we find strong indications that the source of the third harmonic is the optical nonlinearity of the bare gold enhanced by the resonant plasmonic polarization.

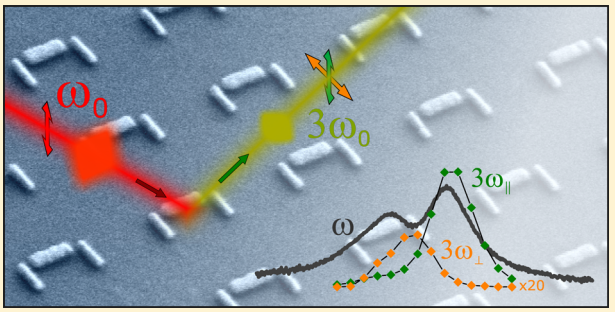

KEYWORDS: *nano optics, plasmonics, nonlinear optics, spectroscopy, third harmonic generation, Fano resonance*

Plasmonic nanostructures are attractive for nonlinear optics, as they resonantly enhance nonlinear effects on the nanoscale.[1] In the last years, scientists just started to design complex plasmonic nanostructures to amplify nonlinear optical processes, such as second and third harmonic (TH) generation or four wave mixing by using doubly resonant or multiresonant antennas[2−5] or plasmonic Fano resonances.[6−8] The latter mainly benefit from a narrow subradiant linewidth, which renders them highly attractive for enhanced optical nonlinearities.[9,10] Recently, a number of detailed studies of the nonlinear optical response of metal nanostructures have been carried out.[11−19] Despite the variety of sophisticated experiments, the microscopic source of the nonlinear response has not been answered conclusively.[20,21] Furthermore, if and under which conditions plasmonic Fano resonances allow for more efficient nonlinear light generation is still under discussion. In this Letter we examine the origin of the nonlinear response of complex plasmonic Fano resonances by polarization-resolved TH spectroscopy of gold dolmen-type nanostructure arrays,[22−24] see Figure 1a. Our results indicate whether it is possible to further enhance nonlinear optical processes using plasmonic Fano resonances and allow drawing conclusions on the source of the TH response.

The investigated gold nanostructure arrays with an area of $100 \times 100\ \mu m^2$ are fabricated via electron beam lithography on a fused silica substrate. The dolmen-type structures consist of a dipole rod placed between two orthogonal oriented dipole rods. In Figure 1b, tilted scanning electron micrographs (SEM) of the fabricated nanostructures are shown. Figure 1c depicts the corresponding geometrical parameters.

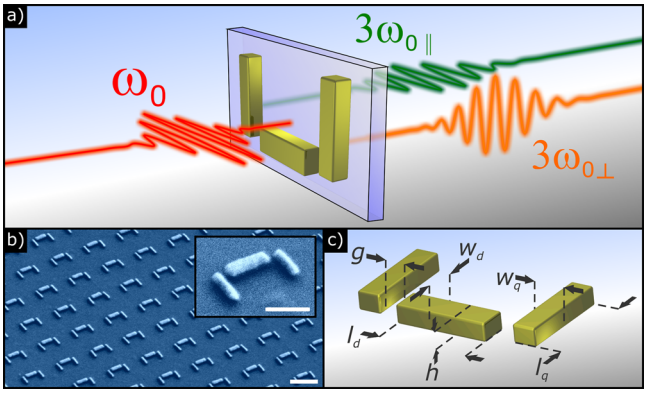

Figure 1. (a) Illustration of TH spectroscopy of plasmonic Fano structures. (b) Tilted SEM images of the samples. The scale bars are 500 and 200 nm in the overview and the inset, respectively. (c) Geometrical parameters of the dolmen-type nanostructures: l_d = 220 nm, w_d = 70 nm, l_q = 190 nm, w_q = 50 nm, g = 40−60 nm, h = 60 nm. The lattice constants of the nanostructure arrays are 600 and 700 nm perpendicular and parallel to the dipole rod, respectively.

Particle plasmons are excited when illuminating the nanostructures with light polarized parallel to the single dipole. Simultaneously, energy is exchanged via the optical near-fields between the dipole and the perpendicularly oriented gold rods. Due to the out-of-phase oscillation of the perpendicularly

Received: February 27, 2014
Published: May 2, 2014

oriented rods they form a subradiant quadrupolar mode. The interference of the bright dipole and the dark quadrupole mode leads to the typical Fano lineshape in the linear extinction spectrum, as shown in Figure 2a, which is characterized by a

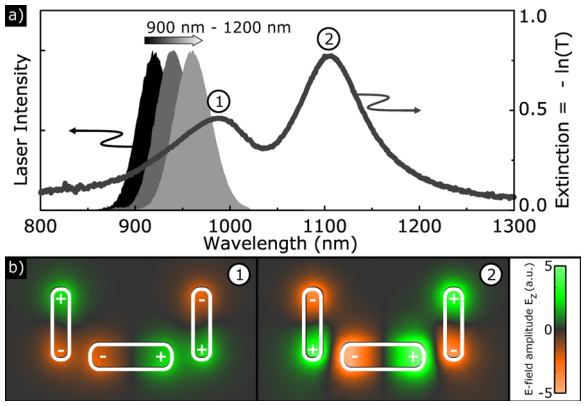

Figure 2. (a) Measured extinction spectrum of a dolmen-type nanostructure array as well as experimental laser spectra, which are tuned over the Fano resonance to measure the TH spectrum of the structure. (b) Simulations of the *z*-component (normal to the substrate) of the electric near-field amplitude 20 nm above the structure at the two spectral positions marked in (a).

spectrally narrow transmittance window within a broad absorbance peak.[9,22−24] The Fano interference results in the formation of two distinct absorption peaks. In Figure 2b, the *z*-components of the electric near-field at the far-field spectral positions of the two peaks are depicted, which were simulated using finite element methods (FEM; Comsol Multiphysics). The near-fields show antisymmetric and symmetric electric field distributions, with repulsive and attractive interaction at the gap region of the structure, respectively.

In order to unravel the nonlinear optical response of the dolmen-type structures we perform polarization-resolved TH spectroscopy experiments. We focus sub-30 fs laser pulses with an average power of about 15 mW, tunable from 900 to 1200 nm (Figure 2a) from an amplitude and phase adjustable pulse shaper,[25] with a 75 mm focal length achromatic lens on the nanostructure arrays. This leads to a beam diameter in the focus of about 50 μm and to peak intensities on the order of about 0.5 GW/cm^2. A factor of 2−3 above these light intensities we could observe slight changes in the linear optical spectra, in particular, after long exposure times. Hence, the damage threshold for the resonantly excited gold nanostructures is located close or slightly above a peak intensity of about 1 GW/cm^2. In order to position the nanostructure arrays in the focus of the exciting laser light, the sample is mounted on an *xyz*-translation stage. Throughout the manuscript, the polarization of the incoming laser light is oriented along the dipole. The TH signals, which are radiated in forward direction, are recollimated with a fused silica lens of the same focal length. Hence, we only collect the zeroth diffraction order of the radiated TH signals, although higher diffraction orders are allowed at the TH frequency, due to the lattice constants of 600 and 700 nm of the nanostructure arrays. Subsequently, the TH signals are analyzed by a polarizer and measured with a Peltier cooled CCD camera attached to a spectrometer.

The experimental results of the TH spectroscopy measurements are shown in Figure 3 in the left column. To examine the influence of the quadrupole on the TH response we varied the gap distance *g* between the dipole and the quadrupole rods from about 60 nm to about 40 nm from top to bottom. Even though the difference in the gap distance *g* is relatively small, the increased coupling is clearly visible in the measured linear extinction spectra as more pronounced splitting of the Fano resonance peaks. In addition to the linear extinction spectra, the integrated TH intensities are depicted over the fundamental wavelength as data points (polarizations: green: ∥ dipole, orange: ⊥ dipole). The TH polarized parallel to the dipole is found to always peak close to the low energy peak of the Fano resonance. Neither in the Fano resonance dip nor at the high energy peak strong TH emission is observed. Perpendicular to the dipole, only very weak TH emission can be detected. For the intermediate gap distance of 50 nm the inset shows the magnified TH perpendicular to the dipole, which we find to peak close to the Fano resonance dip.

In order to unravel the underlying physical mechanisms, we describe the particle plasmons as classical coupled oscillators with a small cubic perturbation, which accounts for the TH

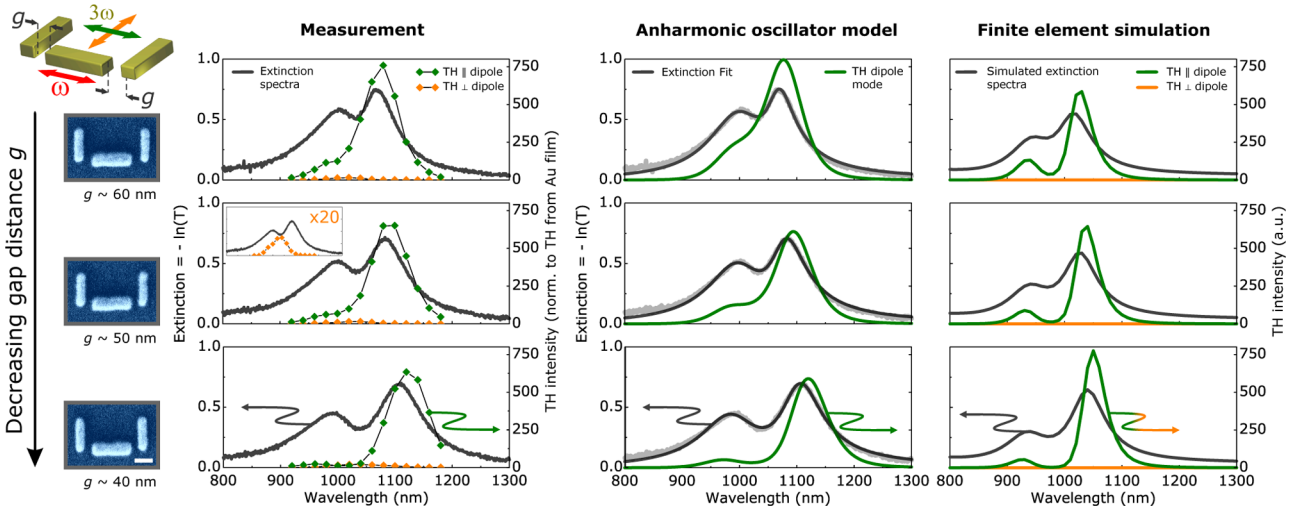

Figure 3. Measured, modeled, and simulated TH spectra plotted together with their corresponding linear extinction spectra for decreasing gap distance *g* from top to bottom. On the left SEM images are depicted, respectively. The scale bar is 100 nm.

dx.doi.org/10.1021/ph5000677 | ACS Photonics 2014, 1, 471−476

generation.[26] Furthermore, we perform FEM simulations to gain more insight on the nonlinear light generation. Both strategies show excellent agreement with our measurements and provide complementary information on the nonlinear optical response of plasmonic nanostructures.

In the anharmonic coupled oscillator model we treat the bright mode of the dipole and the dark mode of the quadrupole rods as classical harmonic oscillators:

$$\ddot{x}_\mathrm{d} + 2\gamma_\mathrm{d}\dot{x}_\mathrm{d} + {\omega_\mathrm{d}}^2 x_\mathrm{d} - \kappa \cdot x_\mathrm{q} + a \cdot {x_\mathrm{d}}^3 = -\frac{e}{m}E(t) \quad (1)$$

$$\ddot{x}_\mathrm{q} + 2\gamma_\mathrm{q}\dot{x}_\mathrm{q} + {\omega_\mathrm{q}}^2 x_\mathrm{q} - \kappa \cdot x_\mathrm{d} + a \cdot {x_\mathrm{q}}^3 = 0 \quad (2)$$

The indices j = d and q represent the dipole and the quadrupole, respectively. Here, $x_j(t)$ is the displacement of the mode, γ_j and ω_j denote its damping and its resonance frequency, κ describes the coupling strength between both modes, the small perturbation parameter a determines the absolute strength of the TH, e and m correspond to the charge and the mass of the dipole oscillator, and $E(t)$ is the electric field of the 30 fs laser pulses. Due to the relatively large gap distances of the structures, we utilize a complex coupling coefficient $\kappa = |\kappa| \cdot e^{i\phi}$, which accounts for the retarded interaction of both modes.[27] The solution of the coupled differential equations can be obtained in the frequency domain using perturbation theory. The unperturbed solution for the displacements $x_{j0}(\omega)$ then follow from a matrix inversion:

$$\begin{bmatrix} x_{\mathrm{d}0} \\ x_{\mathrm{q}0} \end{bmatrix} = -\frac{e}{m}\frac{1}{1 - \kappa^2 g_\mathrm{d} g_\mathrm{q}}\begin{bmatrix} g_\mathrm{d} & \kappa g_\mathrm{d} g_\mathrm{q} \\ \kappa g_\mathrm{d} g_\mathrm{q} & g_\mathrm{q} \end{bmatrix}\begin{bmatrix} E(\omega) \\ 0 \end{bmatrix} \quad (3)$$

Here $g_j(\omega) = -[\omega^2 - \omega_j^2 + 2i\gamma_j\omega]^{-1}$ is the linear response function of an individual oscillator. From the solution, the linear extinction $\alpha(\omega)$ for light polarized along the dipole can be derived.[24,27] Fitting of the measured linear extinction spectra with the expression for $\alpha(\omega)$ yields the linear optical properties (ω_j, γ_j, κ) of the coupled oscillator system. Subsequently, the solution in first order perturbation $x_{j1}(\omega)$, which describes the TH response, can be calculated as $x_{j1}(\omega) \sim \mathcal{F}[x_{j0}(t)^3]$. In this ansatz, cross-terms, which describe the transfer of TH energy between both modes, as well as the linear response function at the TH frequency have been neglected since they are small and spectrally flat, respectively. Hence, in the oscillator model the sources of the nonlinearity are the displacements $x_{j0}(\omega)$ of the unperturbed solution. The expression for $x_{d1}(\omega)$ now allows to calculate the radiated TH from the dipole.[12,13,28]

The results of the anharmonic coupled oscillator model are depicted in Figure 3 in the center column. The TH radiated from the dipole (green) is shown together with the fitted linear extinction spectra (black). The model describes all features of the radiated TH polarized parallel to the dipole for all measured gap distances. In particular, the peak position of the TH is as well found close to the low energy peak. Hence, the TH parallel to the dipole is completely described by the TH of the dipole mode. The TH from the mode of the quadrupole rods is predicted by the model to peak between the Fano resonance dip and the low energy peak (not shown). However, the oscillator model is apparently not capable to describe the "brightness" of the mode of the quadrupole rods and how efficient the mode radiates TH into the far-field. The spectral position however suggests that the weak TH harmonic measured perpendicular to the dipole stems from the quadrupole rods. This matter will be discussed later in the manuscript.

To examine the microscopic source of the TH in more detail we also perform FEM simulations (Comsol Multiphysics) of the dolmen-type structures, which are shown in the right column of Figure 3. In the simulations the structures are defined with the dimensions given in Figure 1c, are positioned on a substrate with a constant refractive index of n = 1.5, and for the optical properties of gold we use the data of Johnson and Christy.[29] For the TH spectra we calculate at each spatial coordinate inside the dolmen-type structures a local TH polarization $\mathbf{P}_{\mathrm{THG,loc}} \sim \chi^{(3)}_{\mathrm{Au}}{\mathbf{E}_{\mathrm{loc}}}^3 \sim [\chi^{(1)}_{\mathrm{Au}}]^3\,{\mathbf{E}_{\mathrm{loc}}}^3 \sim {\mathbf{P}_{\mathrm{loc}}}^3$ from the complex polarization $\mathbf{P}_{\mathrm{loc}}(\mathbf{r}, \omega)$. Here $\mathbf{E}_{\mathrm{loc}}$ is the complex local electric field and $\chi^{(1)}_{\mathrm{Au}}$ and $\chi^{(3)}_{\mathrm{Au}}$ are the first and third order susceptibilities of bare gold, respectively. After the second approximate sign, we used the classical expression of the third order susceptibility, which is proportional to the third power of the fundamental susceptibility[26] (field distributions of the TH polarization in the dolmen-type structures can be found in Figure S1). Finally we integrate over the volume V of the gold structures:

$$\mathbf{E}_{\mathrm{THG}}(\omega) \sim \omega_{\mathrm{THG}} \int_V \mathbf{P}_{\mathrm{loc}}(\mathbf{r}, \omega)^3 \mathrm{d}r^3 \quad (4)$$

In the simulation the sources of the optical nonlinearity are the local polarizations $\mathbf{P}_{\mathrm{loc}}(\mathbf{r}, \omega)$ at each spatial coordinate $\mathbf{r}$ in the gold structures. Since the polarization enters as a complex quantity, the complete phase information is included. Thus, from the simulation we obtain the full polarization state of the complex TH electric field $\mathbf{E}_{\mathrm{THG}}(\omega)$ radiated into the far-field. The TH spectra are then calculated as the intensity $I_{\mathrm{THG}}(\omega)$ of the TH electric field amplitude $\mathbf{E}_{\mathrm{THG}}(\omega)$ in the respective polarization direction. Just like the oscillator model, the simulation predicts the TH polarized parallel to the dipole to peak close to the low energy peak of the Fano resonance (green). The slight differences at the high energy peak, where the simulation shows a small peak instead of a little shoulder, mainly stem from the fact that the simulation is carried out in continuous wave excitation, which does not account for the finite spectral width of the 30 fs laser pulses. In the oscillator model, we accounted for the spectral width of about 45 nm (fwhm) of the laser pulses, which slightly blurs out the features in the TH response. Additionally, the simulation predicts zero TH signal polarized perpendicular to the dipole (orange) due to the symmetry of the structure. The small TH in this polarization direction, which we observe in the experiment, is most likely due to small structure imperfections.

To further examine the origin of the TH radiation polarized perpendicular to the dipole, we now shift the dipole of the structure with 50 nm gap distance in small steps from its center position closer to one of the quadrupole wires (SEM images in Figure 4a). The introduced asymmetry leads to an unequal coupling between the dipole rod and the perpendicularly oriented rods. Hence, the two quadrupole rods are now excited with different strength and phase (due to the distance-dependent retarded coupling). Both effects render the previously dark mode of the quadrupole rods with increased symmetry breaking more bright and dipole-like and, hence, lead to increased radiative damping.

The corresponding TH spectroscopy measurements are depicted in Figure 4a, where the measured TH signals polarized perpendicular to the dipole (orange) together with the measured linear extinction spectra (black) are shown with

dx.doi.org/10.1021/ph5000677 | ACS Photonics 2014, 1, 471−476

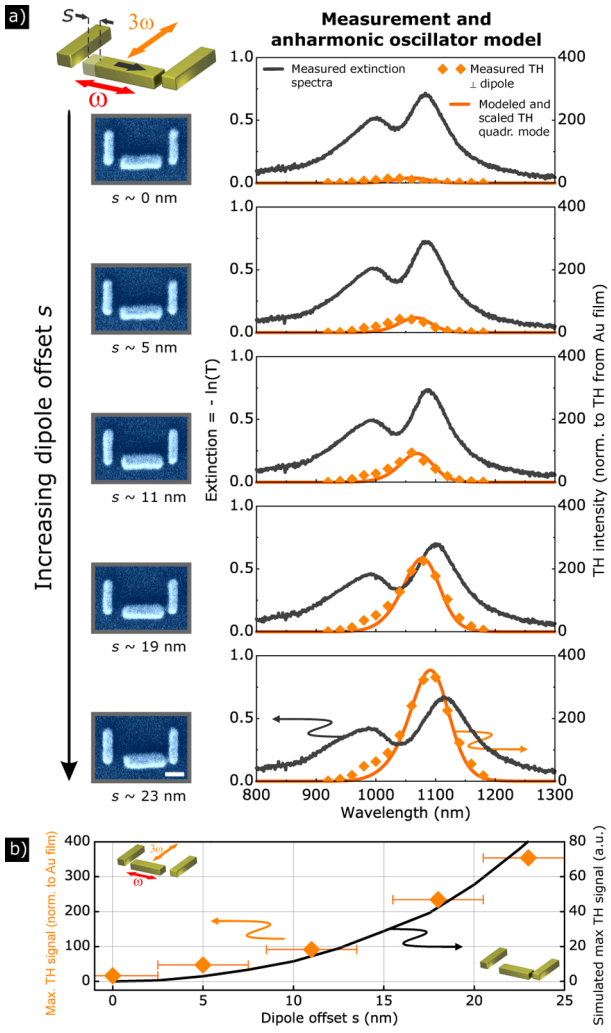

Figure 4. (a) Measured TH spectra polarized perpendicular to the dipole antenna for increasing dipole offset s together with corresponding linear extinction spectra from top to bottom. On the left, SEM images are depicted, respectively. The scale bar is 100 nm. (b) Measured and simulated maximum TH efficiency perpendicular to the dipole antenna for increasing dipole offset s.

increasing dipole offset from top to bottom (see Figure S2 for the corresponding TH signals polarized parallel to the dipole). We find a monotonic increase of the TH emission with increasing dipole offset s. As before, we fitted the linear extinction spectra with the coupled oscillator model and calculated subsequently the displacement $x_{q1}(\omega)$ describing the TH of the mode of the quadrupole rods, see Figure 4a (orange lines). It is noteworthy that only in the fully symmetric case the plasmonic mode of the quadrupole rods is a pure quadrupolar mode. As soon as the symmetry is broken by displacing the dipole wire, the excited mode in the quadrupole rods x_q will be a superposition of the dark quadrupolar mode and a dipole-like contribution. As mentioned before, the oscillator model does not include information about how efficient the mode of the quadrupole rods x_q radiates TH light into the far-field. In contrast to the spectral behavior the absolute far-field TH strength is a parameter that cannot be predicted by the model. Therefore, the modeled TH spectra are scaled with respect to amplitude to the measured TH data points. Nevertheless, the spectral behavior and the peak position of the TH is very well predicted by our simple model.

Furthermore, we simulated the symmetry-broken dolmen-type structures with the FEM and extracted the maxima of the radiated TH intensities perpendicular to the dipole for different dipole offset s. The result is shown in Figure 4b together with the maxima of the measured TH intensities and confirms the monotonic increase of the TH with increasing dipole offset s (see Figure S3 for the complete simulated TH spectra).

We conclude that for the symmetric structure the TH polarization of the mode of the quadrupole rods interferes destructively in the far-field due to the out-of-phase oscillation in the two quadrupole wires. For increasing dipole offset s, the unequal excitation of the quadrupole wires leads to reduced destructive interference and, hence, to efficient radiation of the TH light into the far-field.

The obtained results allow several conclusions on the TH response of plasmonic nanostructures. Our model and the simulations require a normalization of the experimental TH spectra to the off-resonant TH of a bare gold film.[30] This normalization accounts for a wavelength dependent TH response of the bare gold which is explicitly not included in our model and the simulation. We find that the TH of the bare gold changes in the considered wavelength range by about a factor of 3 when comparing it to the TH we obtain from a bare fused silica substrate (see Figure S4). More importantly, we identify the source of the nonlinearity in the oscillator model and the simulation to be the displacement $x_{j0}(\omega)$ and the polarization $\mathbf{P}_{loc}(\mathbf{r},\omega)$, respectively. Both are related in the Lorentz–Drude model via $P = -en_e \cdot x$ and do, in fact, describe the same physical quantity. We conclude that the source of the TH response in plasmonic nanostructures is most likely the bare gold nonlinearity, which is driven and enhanced by the resonant plasmonic polarization $\mathbf{P}_{loc}(\mathbf{r},\omega)$.

At last, we ask whether plasmonic Fano resonances allow for enhanced TH generation in comparison to simple plasmonic dipole antennas. In our experiment the maximum TH light polarized parallel to the dipole increases slightly with decreasing coupling between the dipole and the quadrupole. This is as well confirmed by our oscillator model, which predicts the strongest TH response for a very small coupling coefficient κ, which is equivalent to an isolated dipole. We also observed in experiment that dipole antennas can be more efficient in terms of TH generation than the dolmen-type Fano structures (see Figure S5).

However, a further increase of the lifetime of the dark mode by a factor of 2, which is a crucial parameter for the TH response, is predicted by the model to lead to the doubling of the TH intensity from the dipole mode compared to the TH from isolated dipole antennas. Simultaneously, the TH intensity of the dark mode should be enhanced by over half an order of magnitude. It might be possible to increase this lifetime by using improved structure geometries or by utilizing silver instead of gold for the quadrupole wires, since it exhibits a lower intrinsic damping. Beyond that, it could be promising to resonantly couple other systems, such as excitonic or molecular systems, which intrinsically exhibit quite long lifetimes, to plasmonic dipole antennas and create narrow Fano resonances.[31] This way one could facilitate the required lifetime reduction of the dark mode. This implies that plasmonic Fano resonances instead of simple plasmonic dipole antennas can give extra nonlinearity enhancement, however only for carefully designed structures.

In conclusion, we performed TH spectroscopy of plasmonic dolmen-type nanostructures, that exhibit plasmonic Fano

dx.doi.org/10.1021/ph5000677 | ACS Photonics 2014, 1, 471–476

resonances in their linear extinction spectrum. The TH light polarized parallel to the dipole was found to peak close to the low energy peak of the Fano resonance and originates from the dipole rod. The TH polarization of the subradiant mode interferes destructively in the far-field due to the out-of phase oscillation of the two quadrupolar wires at the fundamental frequency. In fact, similar to this manuscript it was found in fishnet metamaterials that the TH angular radiation pattern can be explained by the constructive and destructive interference of TH sources originating from antisymmetric charge oscillations.[32] Furthermore, the comparison of experimental TH spectra with an anharmonic oscillator model and FEM simulations shows strong indications for the TH response of plasmonic Fano structures to be the optical nonlinearity of the bare gold driven and enhanced by the resonant plasmonic polarization $\mathbf{P}_{loc}(\mathbf{r},\omega)$.

■ ASSOCIATED CONTENT

Supporting Information

Figure S1, simulated field distributions of the TH polarization in dolmen-type nanostructures. Figure S2, measured TH spectra polarized parallel (green) and perpendicular (orange) to the dipole antenna for increasing dipole offset *s*. Figure S3, simulated TH spectra for increasing dipole offset *s*. Figure S4, measured TH spectroscopy of a plane gold film. Figure S5, measured TH response of dolmen-type nanostructures in comparison to plasmonic dipole antennas. Figure S6, tabulated data of the fitted linear optical parameters of the coupled oscillator model. This material is available free of charge via the Internet at http://pubs.acs.org.

■ AUTHOR INFORMATION

Corresponding Author

*E-mail: b.metzger@physik.uni-stuttgart.de.

Notes

The authors declare no competing financial interest.

■ ACKNOWLEDGMENTS

We gratefully acknowledge financial support from the Baden-Württemberg Stiftung (Kompetenznetz Funktionelle Nanostrukturen), from the DFG (SPP1391, ultrafast nanooptics), from the BMBF (13N10146), and the ERC (Complexplas).

■ REFERENCES

(1) Kauranen, M.; Zayats, A. V. Nonlinear Plasmonics. *Nat. Photonics* **2012**, *6*, 737.

(2) Thyagarajan, K.; Rivier, S.; Lovera, A.; Martin, O. J. F. Enhanced Second-Harmonic Generation from Double Resonant Plasmonic Antennae. *Opt. Express* **2012**, *20*, 12860.

(3) Aouani, H.; Navarro-Cia, M.; Rahmani, M.; Sidiropoulos, T. P. H.; Hong, M.; Oulton, R. F.; Maier, S. A. Multiresonant Broadband Optical Antennas As Efficient Tunable Nanosources of Second Harmonic Light. *Nano Lett.* **2012**, *12*, 4997.

(4) Harutyunyan, H.; Volpe, G.; Quidant, R.; Novotny, L. Enhancing the Nonlinear Optical Response Using Multifrequency Gold-Nanowire Antennas. *Phys. Rev. Lett.* **2012**, *108*, 217403.

(5) Navarro-Cia, M.; Maier, S. A. Broad-Band Near-Infrared Plasmonic Nanoantennas for Higher Harmonic Generation. *ACS Nano* **2012**, *6*, 3537.

(6) Thyagarajan, K.; Butet, J.; Martin, O. J. F. Augmenting Second Harmonic Generation Using Fano Resonances in Plasmonic Systems. *Nano Lett.* **2013**, *13*, 1847.

(7) Abb, M.; Wang, Y.; Albella, P.; de Groot, C. H.; Aizpurua, J.; Muskens, O. L. Nonlinear Control of High-Order Modes in Single Asymmetric Nanoantennas. *ACS Nano* **2012**, *6*, 6462.

(8) Zhang, Y.; Wen, F.; Zhen, Y.-R.; Nordlander, P.; Halas, N. J. Coherent Fano Resonances in a Plasmonic Nanocluster Enhance Optical Four-Wave Mixing. *Proc. Natl. Acad. Sci. U.S.A.* **2013**, *110*, 9215.

(9) Luk'yanchuk, B.; Zheludev, N. I.; Maier, S. A.; Halas, N. J.; Nordlander, P.; Giessen, H.; Chong, C. T. The Fano Resonance in Plasmonic Nanostructures and Metamaterials. *Nat. Mater.* **2010**, *9*, 707.

(10) Stockman, M. I. Dark-Hot Resonances. *Nature* **2010**, *467*, 541.

(11) Hanke, T.; Cesar, J.; Knittel, V.; Trügler, A.; Hohenester, U.; Leitenstorfer, A.; Bratschitsch, R. Tailoring Spatiotemporal Light Confinement in Single Plasmonic Nanoantennas. *Nano Lett.* **2012**, *12*, 992.

(12) Hentschel, M.; Utikal, T.; Giessen, H.; Lippitz, M. Quantitative Modelling of the Third Harmonic Emission Spectrum of Plasmonic Nanoantennas. *Nano Lett.* **2012**, *12*, 3778.

(13) Metzger, B.; Hentschel, M.; Lippitz, M.; Giessen, H. Third-Harmonic Spectroscopy and Modeling of the Nonlinear Response of Plasmonic Nanoantennas. *Opt. Lett.* **2012**, *37*, 4741.

(14) Linden, S.; Niesler, F. B. P.; Förstner, J.; Grynko, Y.; Meier, T.; Wegener, M. Collective Effects in Second-Harmonic Generation from Split-Ring-Resonator Arrays. *Phys. Rev. Lett.* **2012**, *109*, 015502.

(15) Czaplicki, R.; Husu, H.; Siikanen, R.; Mäkitalo, J.; Kauranen, M.; Laukkanen, J.; Lehtolahti, J.; Kuittinen, M. Enhancement of Second-Harmonic Generation from Metal Nanoparticles by Passive Elements. *Phys. Rev. Lett.* **2013**, *110*, 093902.

(16) Kim, E.; Wang, F.; Wu, W.; Yu, Z.; Shen, Y. R. Contribution of the Electric Quadrupole Resonance in Optical Metamaterials. *Phys. Rev. B* **2008**, *78*, 113102.

(17) Kujala, S.; Canfield, B. K.; Kauranen, M.; Svirko, Y.; Turunen, J. Multipole Interference in the Second-Harmonic Optical Radiation from Gold Nanoparticles. *Phys. Rev. Lett.* **2007**, *98*, 167403.

(18) Klein, M. W.; Tritschler, T.; Wegener, M.; Linden, S. Lineshape of Harmonic Generation by Metallic Nanoparticles and Metallic Photonic Crystal Slabs. *Phys. Rev. B* **2005**, *72*, 115113.

(19) Klein, M. W.; Wegener, M.; Feth, N.; Linden, S. Experiments on Second- And Third-Harmonic Generation from Magnetic Metamaterials. *Opt. Express* **2007**, *15*, 5238.

(20) Utikal, T.; Zentgraf, T.; Paul, T.; Rockstuhl, C.; Lederer, F.; Lippitz, M.; Giessen, H. Towards the Origin of the Nonlinear Response in Hybrid Plasmonic Systems. *Phys. Rev. Lett.* **2011**, *106*, 133901.

(21) Lippitz, M.; van Dijk, M. A.; Orrit, M. Third-Harmonic Generation from Single Gold Nanoparticles. *Nano Lett.* **2005**, *5*, 799.

(22) Gallinet, B.; Martin, O. J. F. Relation between Near-Field and Far-Field Properties of Plasmonic Fano Resonances. *Opt. Express* **2011**, *19*, 22167.

(23) Zhang, S.; Genov, D. A.; Wang, Y.; Liu, M.; Zhang, X. Plasmon-Induced Transparency in Metamaterials. *Phys. Rev. Lett.* **2008**, *101*, 047401.

(24) Liu, N.; Langguth, L.; Weiss, T.; Kästel, J.; Fleischhauer, M.; Pfau, T.; Giessen, H. Plasmonic Analogue of Electromagnetically Induced Transparency at the Drude Damping Limit. *Nat. Mater.* **2009**, *8*, 758.

(25) Metzger, B.; Steinmann, A.; Giessen, H. High-Power Widely Tunable Sub-20fs Gaussian Laser Pulses for Ultrafast Nonlinear Spectroscopy. *Opt. Express* **2011**, *19*, 24354.

(26) Boyd, R. W. *Nonlinear Optics*, 3rd ed.; Elsevier: New York, 2008.

(27) Taubert, R.; Hentschel, M.; Kästel, J.; Giessen, H. Classical Analogue of Electromagnetically Induced Absorption in Plasmonics. *Nano Lett.* **2012**, *12*, 1367.

(28) Feynman, R.; Leighton, R. B.; Sands, M. *Feynman Lectures on Physics*; Addison-Wesley: Reading, MA, 1977; Vol. *1*, Formula 30.19.

(29) Johnson, P. B.; Christy, R. W. Optical Constants of the Noble Metals. *Phys. Rev. B* **1972**, *6*, 4370.

(30) Bloembergen, N.; Burns, W. K.; Matsuoka, M. Reflected Third Harmonic Generated by Picosecond Laser Pulses. *Opt. Commun.* **1969**, *1*, 195.
(31) Schlather, A. E.; Large, N.; Urban, A. S.; Nordlander, P.; Halas, N. J. Near-Field Mediated Plexcitonic Coupling and Giant Rabi Splitting in Individual Metallic Dimers. *Nano Lett.* **2013**, *13*, 3281.
(32) Reinhold, J.; Shcherbakov, M. R.; Chipouline, A.; Panov, V. I.; Helgert, C.; Paul, T.; Rockstuhl, C.; Lederer, F.; Kley, E.-B.; Tünnermann, A.; Fedyanin, A. A.; Pertsch, T. Contribution of the Magnetic Resonance to the Third Harmonic Generation from a Fishnet Metamaterial. *Phys. Rev. B* **2012**, *86*, 115401.